WORLD CONFERENCE ON TIMBER ENGINEERING 2025
BRISBANE, AUSTRALIA

Advancing Timber for the Future Built Environment

INVESTIGATING THE EFFECTS OF STRAIGHT AND BENT GFRP BARS ON THE FLEXURAL BEHAVIOUR OF GLULAM BEAMS

Catherine Shrimpton[1], Herry Chen[2], Daniel Lacroix[3]

ABSTRACT: This paper presents an overview of the flexural performance of glulam beams reinforced with straight and bent glass-fibre-reinforced-polymer (GFRP) bars. A total of six glulam beams were tested to failure under static loading, including two unreinforced beams and four GFRP-reinforced beams. A comparison and analysis of results between the different reinforcement profiles was conducted to better understand the effects of straight and bent GFRP bars on the flexural behaviour and failure modes of glulam beams. Irrespective of reinforcement type, the addition of GFRP bars contributed to increases in resistance, failure displacement, and stiffness in comparison to unreinforced glulam. Results showed that the change from straight bent GFRP provided slight improvements in maximum resistance and corresponding failure displacement by factors of 1.06 and 1.03, respectively. Additionally, a shift in failure mode from longitudinal shear to flexure was observed for reinforced specimens with straight and bent bars, respectively. A predictive material model was developed and a comparison between the experimental and predicted results is presented.

KEYWORDS: Glulam, Fibre-reinforced polymers, Bent bars, Flexural response

1 – INTRODUCTION

1.1 BACKGROUND

Research efforts on the performance of mass timber products and structural systems has led to major updates in the newest editions of the National Building Code of Canada [1] and International Building Code [2], which now allow for the construction of encapsulated mass timber buildings up to 12- and 18-storeys, respectively.

Despite the progress, there is a lack of design guidelines in both the CSA O86 "Engineering Design in Wood" [3] and the CSA S6 "Canadian Highway Bridge Design Code" [4] addressing the reinforcement and rehabilitation of glued-laminated timber (glulam) beams with fibre-reinforced polymers (FRPs).

The overarching aim of the research program is to provide guidance on the detailing and design of FRP-reinforced wood members and develop tools to better understand and predict their behaviour.

1.2 PREVIOUS RESEARCH

Several types of FRPs exist and can be applied to wood (e.g., sawn timber, glulam) with the purpose of strengthening deficient structural members, retrofitting against extreme hazards (e.g., earthquakes, blast loading), or to be used as a hybrid product in a new design. Common FRP types include glass-FRP (GFRP), carbon-FRP (CFRP), aramid-FRP (AFRP), or basalt FRP (BFRP). These types can be installed through external bonding of FRP sheets [e.g., 5–7] or insertion of FRP bars or plates into the members [e.g., 8,9]. In general, whether in the form of sheets or bars, FRP generally contributes to an overall increase in stiffness and strength with a suggested upper limit of 3% reinforcement to wood area.

Previous research has shown that the location of FRP termination can cause a shift in failure mode from an initial flexural failure of the wood in the maximum moment region to one that is dominated by longitudinal shear and stress concentrations at the FRP termination point [10]. A common issue observed with FRP sheets used as simple tension reinforcement is the premature debonding of the FRP [6,11–13]. Although past research

[1] Catherine Shrimpton, Department of Civil and Environmental Engineering, University of Waterloo, Waterloo, Canada, ceshrimp@uwaterloo.ca

[2] Herry Chen, Department of Civil and Environmental Engineering, University of Waterloo, Waterloo, Canada, herry.chen@uwaterloo.ca

[3] Daniel Lacroix, Department of Civil and Environmental Engineering, University of Waterloo, Waterloo, Canada, daniel.lacroix@uwaterloo.ca

https://doi.org/10.52202/080513-0599

conducted on wooden beams reinforced with straight bars have not reported premature debonding to be an issue [9,14], it is hypothesized that debonding can occur due to the wood pushing outwards as it fails in flexure. [6,11–13].

1.3 OBJECTIVES

The current paper focuses on the effects of rebar profile (i.e., bent vs. straight). The potential of bent bars inserted partially through the beam depth and reinforcement length as a measure to prevent potential debonding with straight bars and as observed in the specimens reinforced with simple tension fabric reinforcement. A predictive material model is developed and used to compare the analytical resistance curves to the experimental curves.

2 – PROJECT DESCRIPTON

The experimental program included the testing of six glulam beams, two of which being unreinforced and four having GFRP bar reinforcement. The glulam specimens used in this study were of stress grade 24F-ES and the specimen lengths were determined in accordance with ASTM D198 "Standard Test Methods of Static Tests of Lumber in Structural Sizes" [15]. Final cross-sections of 137 mm x 241 mm x 2,800 mm were chosen for the beams, having a depth to width ratio of 1.75:1. Prior to testing the specimens were stored in a humidity chamber, allowing for the specimens to remain at an average moisture content of 11% with a coefficient of variation of 0.12. The average density of the beams was determined to be 551 kg/m^3 with a coefficient of variation of 0.02.

Of the six specimens, four beams were reinforced with two GFRP bars as simple tension reinforcement (Fig. 1). The reinforcement schemes varied in bar configuration (i.e., straight versus bent). The GFRP bars were No. 6 bars, having a diameter of 20 mm and length of 2,247 mm and the distance between the FRP termination point and beginning of the support plate was chosen to be 25 mm. The beams were prepared by routing grooves into the tension face of the beams for the bars to be placed. A layer of epoxy primer was first used to saturate the wood prior, after which the bars were placed in the grooves and filled with epoxy. A summary of the test matrix is shown in Table 1.

Table 1: *Test Matrix*

Specimen	Bar Type	Reinforcement Length (mm)	End Distance (mm)
U-1 – U-2	Unreinforced	-	-
RS-1, RS-2	Straight	2247	25
RB-1, RB-2	Bent		

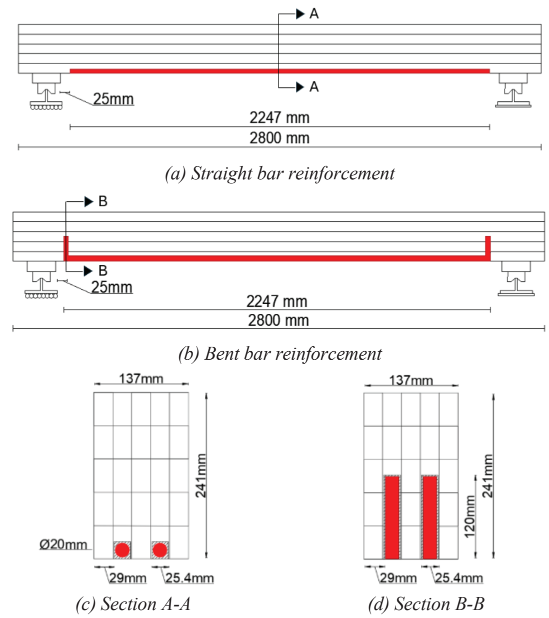

Figure 1: *Reinforcement configurations*

3 – EXPERIMENTAL TEST SETUP

The full-scale tests were conducted in accordance with ASTM D198 [15], where both the unreinforced and GFRP-reinforced beams were tested to failure under four-point bending with simply supported boundary conditions. A 500 kN hydraulic load frame with load cell was used to load all the beams for the bending tests (Fig. 2). The beams were loaded under displacement control with a loading rate of 5 mm/min, to ensure that failure occurred within the first five to ten minutes [15]. The applied load and deflections were measured using the frame load cell and a string pot, respectively. Strain gauges measured the strains at points of interest such as tensile and compressive behaviour of the wood at midspan of the beam and the FRP bar.

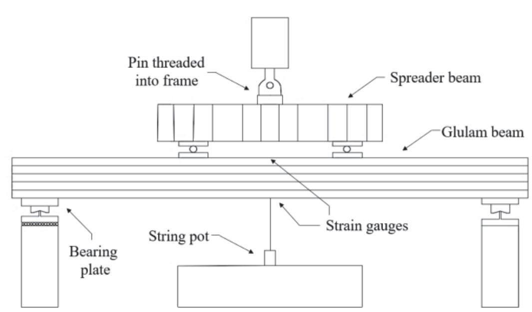

Figure 2: *Test set up*

https://doi.org/10.52202/080513-0599

4 – EXPERIMENTAL RESULTS

4.1 FAILURE MODES

Two unreinforced beams were tested to failure for which the observed failure mode consisted of splintering tension. Fig. 3 shows the splintering tension failure in specimen U-2, where the failure initiated in the maximum moment region and continued to propagate via the path of least resistance in the specimen.

Four beams with GFRP-reinforcement were tested to failure under four-point static bending. The initial failure mode observed for straight bar reinforced specimens (i.e., RS-1, RS-2) was longitudinal shear, and upon further loading secondary failures of simple tension were observed. Fig. 4a shows the initial shear failure that occurred in specimen RS-1, the initial shear failure caused the resistance to decrease by 20%, the test continued reaching a secondary peak resistance prior to a simple tension failure (Fig. 4b) initiating from a defect in an area of high bending stress.

The observed failure modes for the bent bar reinforced beams were splintering tension (i.e., RB-1), and cross-grain tension (i.e., RB-2), The splintering tension failure observed in specimen RB-1 is shown in Fig. 5a. The failure initiated from a finger joint on the tension face of the beam. Specimen RB-2 experienced a brittle cross grain tension failure, (Fig. 5b). A large knot was located on the tension face of beam and is likely responsible for the sudden failure mode of this specimen.

Figure 3: *Splintering tension failure of specimen U-2*

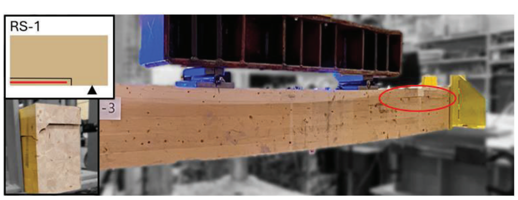

(a) Initial shear failure of beam RS-1

(b) Secondary simple tension failure of beam RS-1

Figure 4: *Representative failures of straight bar reinforced specimens*

(a) Splintering tension failure of beam RB-1

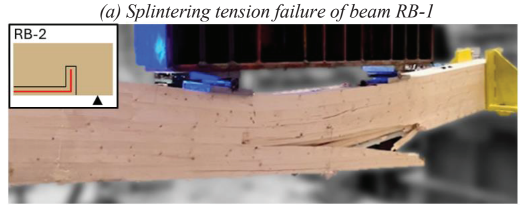

(b) Cross-grain tension failure of beam RB-2

Figure 5: *Representative failures of bent bar reinforced specimens*

4.2 ANALYSIS OF RESULTS

Unreinforced specimens

A summary of the flexural results is presented in Table 2 where key parameters are presented, including the maximum applied load (P_{max}), the corresponding displacement (Δ_{max}) and the initial stiffness (K), defined as the slope from 10 to 40% of the load-displacement curve. The resistance curves for the unreinforced beams are shown in Fig. 6 where the unreinforced specimens are observed to behave linearly up to the maximum load followed by a drop in resistance that is associated with the initial failure. Generally, unreinforced glulam specimens exhibit little to no post-peak resistance as shown in Fig. 6.

Table 2: *Unreinforced Beam Test Results*

Specimen	P_{max} (kN)	Δ_{max} (mm)	K (N/mm)
U-1	167.3	28.9	6,213
U-2	162.4	30.0	5,973
Average	164.9	29.5	6,093

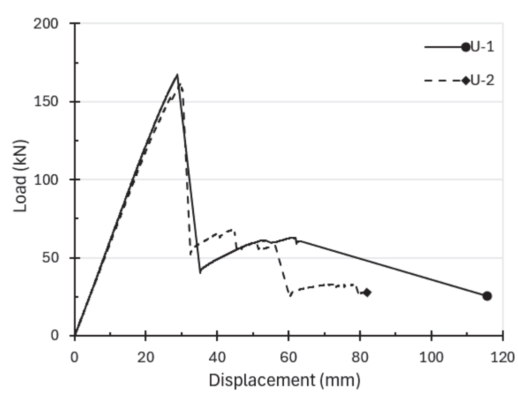

Figure 6: *Resistance curves for unreinforced specimens*

https://doi.org/10.52202/080513-0599

Effects of GFRP reinforcement

A summary of the results for the specimens with GFRP reinforcement is presented in Table 3, including the maximum applied load (P_{max}), the corresponding displacement (Δ_{max}) and the initial stiffness (K) defined as the slope from 10 to 40% of the load-displacement curve.

The resistance curves for the GFRP-reinforced beams are shown in Fig. 7 where the specimens are observed to behave linearly up to the maximum load followed by a drop in resistance associated with the initial failure. The difference in behaviour of specimen RS-1 can be attributed to the initial shear failure that occurred. Irrespective of the reinforcement configuration provided and the failure mode observed, increases in maximum load, displacement at maximum load, and stiffness by factors ranging between 1.22-1.29, 1.18-1.22 and 1.15, respectively, relative to the unreinforced specimens were observed (Fig. 7). Furthermore, an improvement in post-peak behaviour was observed with GFRP-reinforcement.

The addition of straight bars, which corresponded to 1.73% of GFRP reinforcement-to-wood area, contributed to stiffening the beams, allowing for greater loads to be sustained. Therefore, causing a shift in the initial failure from flexure, as observed in the unreinforced beams, to one that is dominated by shear, and then followed by a secondary failure of simple tension upon further loading. The bent bars contributed to similar increases in maximum resistance and stiffness as the straight bars in comparison to the unreinforced specimens. No shear failures were observed for the specimens with bent GFRP bars, suggesting the change from straight to bent reinforcement caused a change in failure mode from one that is dominated by horizontal to shear to flexure.

Table 3: *GFRP-Reinforced Beam Test Results*

Specimen	P_{max} (kN)	Δ_{max} (mm)	K (N/mm)
RS-1	173.1	26.2	7,076
RS-2	229.2	43.6	6,987
Average	201.2	34.9	7,032
RB-1	207.6	35.7	6,832
RB-2	216.9	36.0	7,178
Average	212.3	35.9	7,005

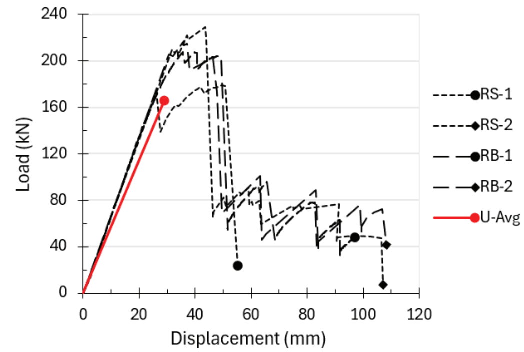

Figure 7: *Resistance curves relative to unreinforced average*

Effects of bar profile

One of the study's hypotheses was that larger distances between the reinforcement termination point and support could result in a failure caused by stress concentrations at the end of the reinforcement akin to those observed in Shrimpton et al. [16]. As such, distances of 25 mm and 125mm between the reinforcement termination point and the support were investigated. In comparison, Shrimpton et al. [16] had a distance of 105.5 mm. Additionally, the effect of bent bars was investigated as a mean to provided increased anchoring at the reinforcement termination point.

The change in bar profile from straight to bent bars provided slight improvement to the maximum load and failure displacement on average by factors of 1.06 and 1.03 respectively, compared to the specimens with straight bars. The change from straight to bent bars resulted in a shift in failure mode from shear to flexure.

For the straight bars, upon initial failure and further loading, slip was observed in the straight bars (Fig. 8a) creating a gap in the groove where they used to sit. On the other hand, the bent bars are observed to yield (Fig. 8b) due to the additional anchoring provided. The additional force provided with the bent bars can be seen in the failure of the wood, which is similar to group-tear-out in bolted connections [3]. Therefore, while having reinforcement as close as possible to the members' end, additional consideration is required in terms of secondary failures modes.

https://doi.org/10.52202/080513-0599

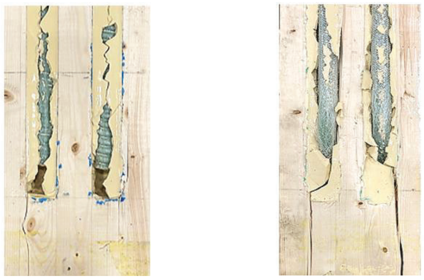

(a) Straight bars *(b) Bent bars*

***Figure 8:** Reinforcement end behaviour*

Effects of GFRP on Strain Behaviour

The full-scale beams were instrumented with two and three strain gauges on the unreinforced and reinforced beams, respectively. The strains at the mid-span of the wood tension and compression face were instrumented, along with one at the midspan of a GFRP bar for the reinforced specimens. Table 5 presents a summary of the strain results for the unreinforced and GFRP-reinforced beams, including the largest recorded wood tensile strains ($\varepsilon_{t,\ max}$), wood compressive strains ($\varepsilon_{c,\ max}$) and FRP bar strains ($\varepsilon_{FRP,\ max}$).

Fig. 9 shows representative load- and strain-displacement diagram for an unreinforced and GFRP-reinforced beam. For the unreinforced (Fig. 9a), the maximum tensile strain coincided with the initial splintering tension failure, after which the strain gauge failed due to its proximity to the failure location (Fig. 3). It can also be seen that upon further loading that the compression strain continued to increase with jumps coinciding with subsequent layers of wood failing with no significant post-peak resistance. For the GFRP-reinforced beam, similar behaviour is observed, with the maximum tensile strain coinciding with the initial failure (Fig. 9b). No improvement in tensile failure strain is observed for the RS specimens in comparison to the unreinforced, which can be attributed to the shear failures that occurred. On average, increases by a factor of 1.5 were observed for the tensile failure strain for the RB specimens compared to the unreinforced.

Table 5: Summary of Strains

Specimen	$\varepsilon_{t,max}$ x 10^{-3} (mm/mm)	$\varepsilon_{c,max}$ x 10^{-3} (mm/mm)	$\varepsilon_{FRP,max}$ x 10^{-3} (mm/mm)
U-1	1.7	-3.7	-
U-2	5.5	-9.6	-
Average	**3.6**	**-6.7**	**-**
RS-1	2.8	-5.4	6.8
RS-2	4.4	-4.7	6.0
Average	**3.6**	**-5.1**	**6.4**
RB-1	5.7	-3.3	11.8
RB-2	3.7	-12.7	11.3
Average	**5.5**	**-7.8**	**11.6**

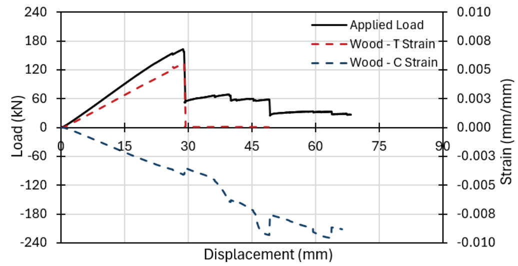

(a) Unreinforced (U-2)

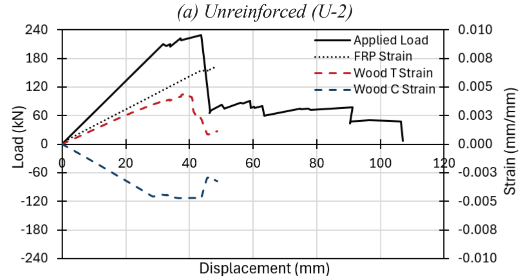

(b) Reinforced (RS-2)

***Figure 9:** Load- and strain-displacement curves*

5 - ANALYTICAL MODELLING

5.1 DESCRIPTION OF ANALYTICAL MODEL

Previous material models for wood were originally developed based on tension being linear elastic and compression being a bilinear stress-strain relationship [17]. The numerical model in the current paper was developed to generate bending moment resistance curves for cross-sections with predefined dimensions and material stress-strain relationships. The moment-curvature relationship was generated until failure by increasing the tensile strain and evaluating the corresponding moment resistance. Failure occurs once the program detects that the material stresses have exceeded the material limits that were determined experimentally. After the moment-curvature relationship has been determined, curvatures are assigned at mid-span and integrated twice to initially obtain rotation along the member's length and ultimately the displacement [13,18].

The material properties used as inputs for the material model were obtained experimental through coupon and non-destructive full-scale testing. The compressive stress-strain relationship is defined by the yield point (f_{cy} = -33.4 MPa, ε_{cy} = -0.0031), ultimate strength (f_{cu} = -27.2, ε_{cu} = -0.017) whereas the tension and stress-strain relationship are defined as linear-elastic with an ultimate failure point (f_t = 51.4 MPa, ε_t = 0.0048). For both the compressive and tensile relationships, a modulus of elasticity of 10,718 MPa corresponding to the mean experimental value is used. The stress-strain relationship of the GFRP was defined as linear elastic with a modulus of elasticity of 60,000 MPa and an ultimate failure stress of 1000 MPa as provided by the manufacturer. Furthermore, two main assumptions were made during the analysis, namely, a perfect bond between the reinforcement and the wood fibres, and only the tensile stresses of the FRP were considered in the cross-section analysis.

5.2 COMPARISON OF ANALYTICAL PREDICTIONS TO EXPERIMENTAL CURVES

A comparison between the average experimental and modelled results in terms of the maximum applied loads (P_{max}) and corresponding displacements (Δ_{max}) of the unreinforced and GFRP-reinforced beams are reported in Table 6. Fig. 10 provides a comparison of the resistance curves and predicted results for the unreinforced and GFRP-reinforced glulam beams.

Table 6: Experimental and Predicted Results

Specimen	Experimental		Model		Model/Exp.	
	P_{max} (kN)	Δ_{max} (mm)	P_{max} (kN)	Δ_{max} (mm)	P_{max} (kN)	Δ_{max} (mm)
U-1, U-2	164.9	29.5	165.5	34.2	1.00	1.16
RS-1, RS-2	201.2	34.9	200.4	48.2	0.99	1.38
RB-1, RB-2	212.3	35.9			0.94	1.34

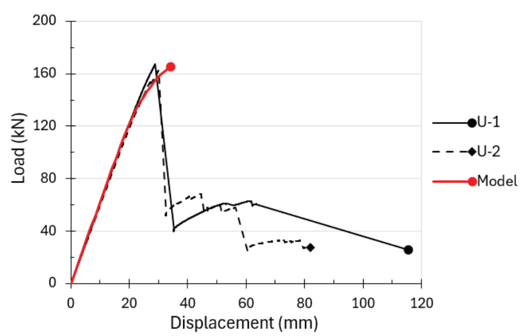

(a) Unreinforced beams

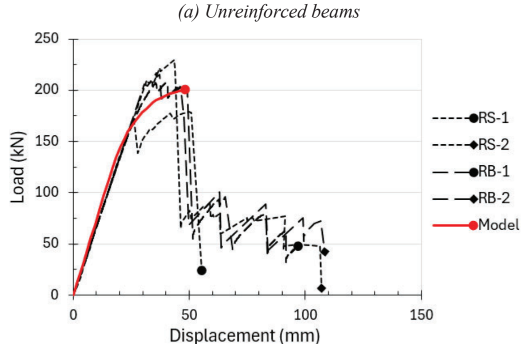

(b) Reinforced beams

Figure 10: *Experimental and modelled resistance curves*

The model predicts the maximum load and stiffness well for both the unreinforced and GFRP-reinforced glulam beams. Ratios between the modelled to experimental results for the maximum loads and failures displacements of 1.00 and 1.16, 0.99 and 1.38, and 0.94 and 1.34, respectively, were seen for the unreinforced, RS and RB specimens. The discrepancies in failure displacement can be attributed to variability in wood properties used as material model inputs.

6 – CONCLUSIONS

The current research program investigated the effects of reinforcement configuration on FRP-reinforced glulam beams. Six glulam beams were tested to failure under four-point static bending, including two unreinforced beams and four beams with GFRP reinforcement purposed to investigate the effects of straight and bent bars. It was observed that irrespective of reinforcement configuration, the addition of GFRP reinforcement provided increases in maximum load, displacement at maximum load, and stiffness relative to unreinforced glulam.

The effects of bent bars were investigated as means of providing increased anchoring at the reinforcement terminations point to prevent the failures caused by stress concentrations observed in simple tension reinforced beams [16]. The effect of bar profile showed that the change from straight to bent bars contributed to improvements by 1.06 and 1.03 with respect to the maximum load and failure displacement, respectively. Additionally, the change from straight to bent bars resulted in a shift in failure mode from shear to flexure. A material model was developed capable to predict the behaviour of unreinforced and GFRP-reinforced glulam beams with reasonable accuracy.

7 – REFERENCES

[1] CCBFC. National Building Code of Canada 2020 2020.

[2] International Code Council. 2021 International Building Code (IBC) | ICC Digital Codes 2021. https://codes.iccsafe.org/content/IBC2021P1 (accessed May 16, 2022).

[3] CSA. Engineering Design in Wood. CSA Group 2024.

[4] CSA. Canadian Highway Bridge Design Code (CSA S6:19). Canadian Standards Association; 2019.

https://doi.org/10.52202/080513-0599

[5] Buell TW, Saadatmanesh H. Strengthening timber bridge beams using carbon fiber. Journal of Structural Engineering 2005;131:173–87. https://doi.org/doi:10.1061/(ASCE)0733-9445(2005)131:1(173).

[6] Johns KC, Lacroix S. Composite reinforcement of timber in bending. Canadian Journal of Civil Engineering 2000;27:899–906. https://doi.org/10.1139/l00-017.

[7] Lacroix D, Doudak G. Towards enhancing the post-peak performance of glued-laminated timber beams using multi-directional fibre reinforced polymers. Eng Struct 2020;215:110680. https://doi.org/10.1016/j.engstruct.2020.110680.

[8] Rajczyk M, Jończyk D. Behavior of glulam beams strengthened with BFRP bars. IOP Conf Ser Mater Sci Eng, 2019. https://doi.org/10.1088/1757-899X/603/4/042004.

[9] Gentile C, Svecova D, Rizkalla H. S. Timber beams strengthened with GFRP bars: Development and applications. Journal of Composites for Construction 2002;6:10. https://doi.org/http://dx.doi.org/10.1061/(ASCE)1090-0268(2002)6:1(11)#sthash.phi4zCIr.dpuf.

[10] Vetter Y. Effects of transverse GFRP reinforcement on the flexural behaviour of glulam beams. Master of Applied Science. University of Waterloo, 2022.

[11] Hernandez R, Davalos F. J, Sonti SS, Kim Y, Moody C. R. Strength and stiffness of reinforced yellow-poplar glued laminated beams. Madison, WI: U.S. Department of Agriculture, Forest Service, Forest Products Laboratory; 1997.

[12] Dorey AB, Cheng JJR. The behavior of GFRP glued laminated timber beams. Montreal: Canadian Society for Civil Engineering; 1996.

[13] Lacroix D, Doudak G. Experimental and analytical investigation of FRP retrofitted glued-laminated beams subjected to simulated blast loading. Journal of Structural Engineering 2018;144. https://doi.org/10.1061/(ASCE)ST.1943-541X.0002084.

[14] Che C. Investigating the effects of glass-fibre-reinforced polymer fabrics and bars on the flexural behaviour of sawn timber and glulam beams. University of Waterloo, 2023.

[15] ASTM. Standard Test Methods of Static Tests of Lumber in Structural Sizes (ASTM D198). West Conshohocken, PA: American Society for Testing and Materials; 2022. https://doi.org/10.1520/D0198-15.

[16] Shrimpton C, Siciliano S, Chen H, Vetter Y, Lacroix D. An Experimental Investigation of Failure Modes in Short-Span FRP Reinforced Glulam Beams. World Conference on Timber Engineering, Oslo, Norway: 2023, p. 1–7.

[17] Buchanan AH. Bending strength of lumber. Journal of Structural Engineering 1990;116:1213–29. https://doi.org/10.1061/(ASCE)0733-9445(1990)116:5(1213).

[18] Lacroix D. Investigating the behaviour of glulam beams and columns subjected to simulated blast loading. University of Ottawa, 2017. https://doi.org/10.20381/ruor-21031.